

Nearest Neighbor Sampling of Point Sets using Random Rays

Liangchen Liu

The University of British Columbia

lewis01@math.ubc.ca

Louis Ly

The University of Texas at Austin

louisly@utexas.edu

Colin Macdonald

The University of British Columbia

cbm@math.ubc.ca

Richard Tsai

The University of Texas at Austin

ytsai@math.utexas.edu

Abstract

We propose a new framework for the sampling, compression, and analysis of distributions of point sets and other geometric objects embedded in Euclidean spaces. A set of randomly selected rays are projected onto their closest points in the data set, forming the RaySense signature. From the signature, statistical information about the data set, as well as certain geometrical information, can be extracted, independent of the ray set. We present promising results from “RayNN”, a neural network for the classification of point clouds based on RaySense signatures.

1. Introduction

We propose a novel method for sampling point clouds or other geometric objects. We call our approach “RaySense” because it samples by firing randomly-chosen rays through the ambient space occupied by the object. At a few points along each ray, we sample the nearest neighbors in the object; the ray senses the structure of the object. We can then work with this data—the *RaySense signature*—instead of the original object, which can be a point cloud, triangulated surface, volumetric representation, etc.

RaySense assumes that the object, Γ , is embedded in a Euclidean space, \mathbb{R}^d using some suitable representation. For example, $d = 3$ for CAD models of a physical object [3, 30], an implicit surface, or a collection of shapes, discretized and represented as black-and-white images. Γ may contain point sets from geometrical objects containing parts of different Hausdorff dimensions; e.g., solids balls interconnected by line segments. In general, RaySense will work on data already transformed into a suitable feature space. In this article, we limit much of the discussion to point sets in \mathbb{R}^3 . We assume the objects to be compared are calibrated, e.g., centered, rotated, and scaled consistently.

When the object is a point cloud, the RaySense samples are easy to find via discrete nearest neighbor searches. There are computationally efficient algorithms for performing nearest-in-Euclidean-distance neighbor searches, for example, tree-based algorithms [2], and grid-based algorithms [27]. For very high dimensions, there is also randomized nearest neighbor search algorithms [9]. We show that certain

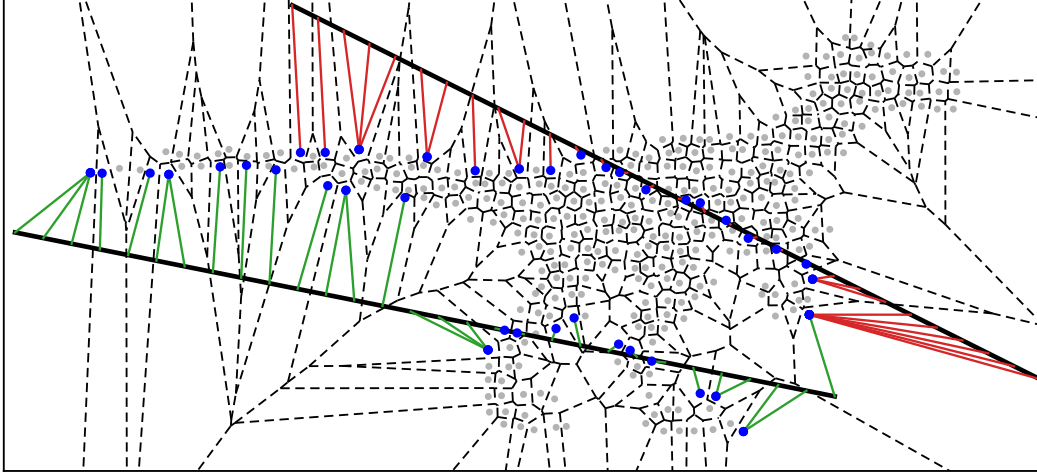


Figure 1: A simple 2D point set (gray). Two rays (black) sense nearest neighbors of the point set (blue). Singular points, such as the tip of the tail, have larger Voronoi cells (dashed lines) and are more likely to be sampled. Closest point pairs are shown in green and red.

statistical information from the sampled data are dependent only on the ray distribution, not specific ray sets.

When the object is a smooth submanifold in \mathbb{R}^d , one can easily extract local geometrical information (such as curvature) from the nearest points of the rays. When Γ is a finite point set on a smooth manifold, curvature information can also be derived from multiple nearest neighbors of each point on the rays.

RaySense has potential applications for *registration*, *classification*, *segmentation*, and *compression* of data. In this article, we consider registration as a pre-processing step that is already applied to the data set, and focus on the problem of classification. The size of the RaySense signature can be predetermined for a collection of data sets, while the cardinality of each member data set may vary. Therefore, the use of RaySense signatures offers flexibility in designing algorithms for comparing data sets of different sizes.

We also demonstrate that RaySense, combined with the proposed neural network, RayNN, performs at least on par with carefully tuned state-of-the-art convolutional neural networks on 3D point cloud classification problems. Intuitive explanations for RaySense’s success include (a) repeated sampling of salient feature points; and (b) some locality and high-order information related to (suitably defined notions) of curvatures.

We draw rays from a distribution \mathcal{P} . Each ray is a line segment in \mathbb{R}^d . We consider k uniformly spaced points along each ray, with spacing δr . With $r_{i,j}$ denoting the j -th point on the i -th ray, we define the RaySense signature tensor $S(\Gamma)$, with entries $[S(\Gamma)]_{i,j} := P_{\Gamma} r_{i,j}$, where $P_{\Gamma} r_{i,j}$ is the nearest point in Γ to $r_{i,j}$. In cases of nonuniqueness, we choose arbitrarily. Later in § 2.2 we generalize the entries of the RaySense signature to live in a “feature space” X by including additional components.

1.1. Snapshots of RaySense features

RaySense signatures For discrete point sets, the likelihood that a ray senses a particular point is related to the Voronoi cell of the point, as we discuss further in § 3. Fig. 1 shows that salient points are more likely to be sensed by a ray due to their larger Voronoi cells. In Fig. 2, we show examples of two rays

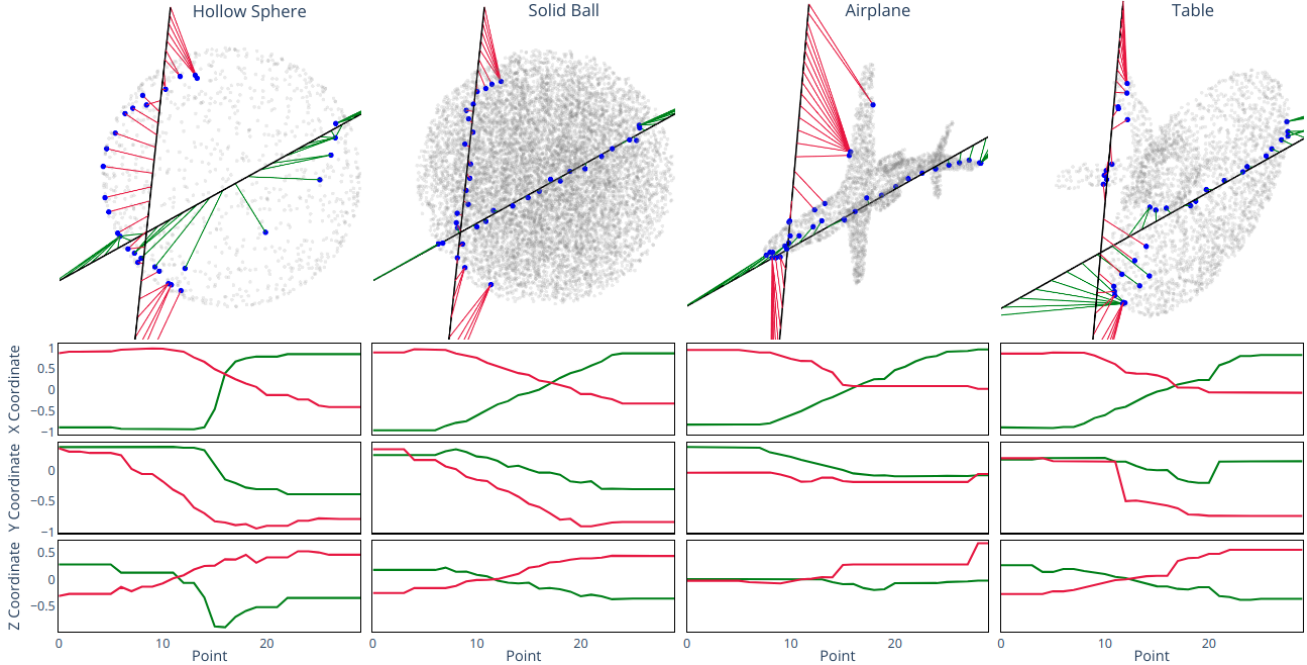


Figure 2: RaySense signatures using 30 sample points per ray. Row 1: visualization of two rays (black) through points sampled from various objects (gray). Closest point pairs are shown in green and red. Rows 2–4: the x , y , and z coordinates of the closest points to the ray.

sensing various 3D point clouds, along with the corresponding features of the signature tensor. Fig. 3 shows how often each point is “sensed” by different rays. Points that are sampled by multiple rays are larger.

Curvature information If the object is a smooth manifold in \mathbb{R}^d (e.g., the sphere in Fig. 2) then each ray induces a parameterized curve $\gamma(t) \in \mathbb{R}^d$. The curvature of $\gamma(t)$ can be approximated by finite differences of consecutive values along the ray. For example, a typical experiment with $\delta r = 0.05$ when Γ is a unit sphere gave values such as 0.99913, 0.99825 and 0.99748, compared to the exact value of one.

Thus even with only a few rays, we obtain local samples of higher-order geometric information. Note the calculations in this example can be performed as combinations of 1×3 convolutions along the ray; thus we can expect RayNN in § 4 to have access to curvature information.

“Coverage” of an object by RaySense Our next experiments look at how well a set of rays “cover” data sets in higher dimensional Euclidean spaces. One way to measure this is to compute the maximum distance from every point in an object Γ to points that contribute to the signature $S(\Gamma)$. The smaller this value, the closer we are to sampling the entire object. We experiment with different point clouds of various dimensions in Fig. 4. Notably, the coverage does not strongly depend on m when the object is inherently lower dimension and merely “rotated” into the higher dimensional space (first column of Fig. 4). If the object is more complicated, we may need more rays to attain the same coverage as the dimension increases (Fig. 4 top-right). Nonetheless, we often obtain coverage that is roughly dimension-independent (Fig. 4 bottom-right).

Data in higher dimensions We consider the MNIST dataset [15], treating each image as a point in $d = 784$ dimensions. Here Γ is point set consisting of all images of the same digit.

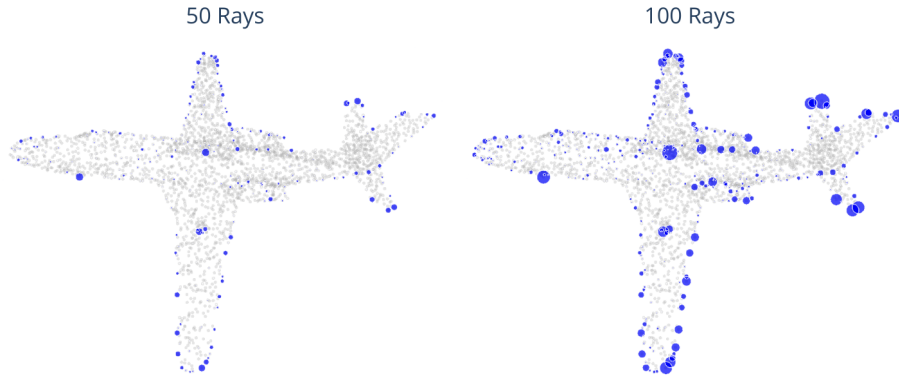


Figure 3: RaySense is more likely to sample salient features in the point cloud. Larger points are repeated more often. We can control the number of points by increasing the number of rays. Each ray contains 30 sample points.

As with the airplane example in Fig. 3, RaySense tends to sample salient points in the data. Fig. 5 shows the average digits over the whole dataset, versus the average of those sampled by RaySense. In the context of MNIST, salient points are digits that are drawn using less typical strokes (according to the data). These are the data points that may be harder to classify, since they appear less frequently in the data. RaySense may be used to determine the most *useful* data points to label, as in active learning [24].

1.2. Related work

In Integral Geometry, one uses the probability of intersection of affine subspaces of different dimensions with the target data manifold to deduce information about the manifold. The interaction information obtained from the “sensing” affine subspaces is binary: yes or no; i.e., $X = \{0, 1\}$. One thus has a counting problem: how frequently will rays intersect with the data manifold. From these probabilities, one may extract geometrical information about the manifold; see e.g., [6]. Nevertheless, this approach may be inefficient in practice.

One may further consider integrating certain information gathered along rays. The Radon transform is a classic example where a local density is integrated along each ray.

Our idea is to add additional dimensions to record information about the data. For example, along a ray, we may store the distance to the closest point in the data. One can draw an analogy to seismic imaging, where designated points on each ray correspond to geophones that record the first arrival time of waves from known sources. One difference is that in seismic imaging, the sensor arrays typically lie on top of the domain of interest—in RaySense, the sensors are placed on rays that penetrate the ambient space.

Abstractly speaking, RaySense is about the mapping of a set of randomly selected rays to some space X that is used to record information about the data. Correspondingly, one designs functions on X to extract information. In RaySense, we propose the use of nearest neighbor information.

From the perspective of the computer vision community, RaySense can be considered a shape descriptor, mapping from 3D point sets to a more informative feature space where point sets can be easily compared. Generally, descriptors try to capture statistics related to local and global features. See [10] for a survey. More recently, researchers have combined shape descriptors with machine learning [4, 22, 26, 31]. RaySense applies more generally to data in arbitrary dimensions.

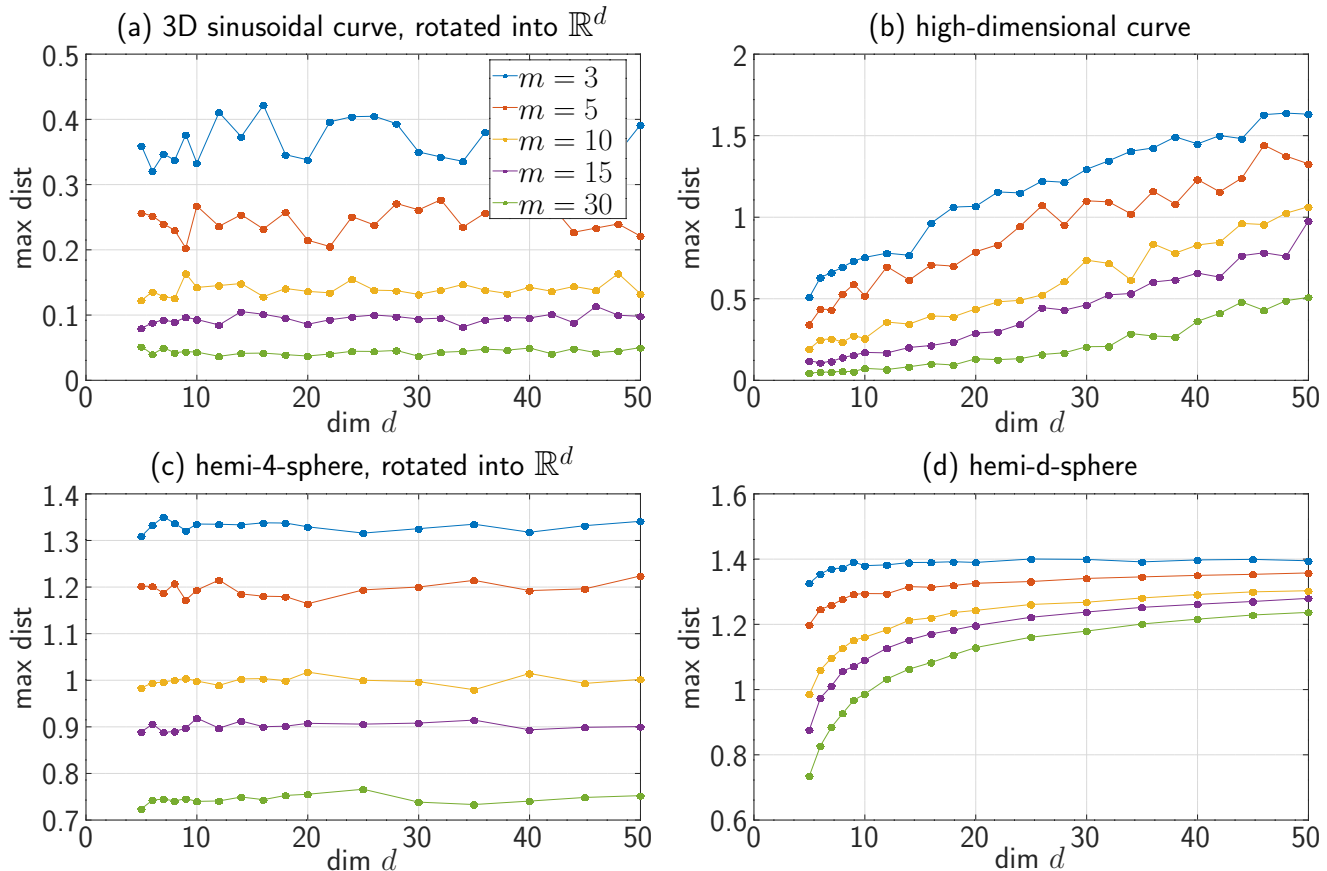


Figure 4: Coverage of point clouds in various dimensions by RaySense using m rays with 32 samples per ray. Top: 5000 points sampled from curves. Bottom: 25000 points sampled from hemispheres. Low-dimensional examples embedded by random rotations into \mathbb{R}^d . Noise of size 10^{-4} added and results averaged over 40 realizations.

Some methods use machine learning directly on the point set to directly learn features for specific tasks, such as classification [1, 12, 16, 20, 21, 25, 28, 29, 32]. Rather than using machine learning on the point set, we use the RaySense signature as input. We show this is more efficient for classification in § 4.

Salient points tend to appear more frequently within the RaySense signature. By retaining only the most frequently repeated points, RaySense resembles keypoint detectors [13] or compression algorithms.

The ray-casting and ray-tracing communities [7, 14, 19] use kd-tree-based algorithms for very efficient computation of nearest-neighbor queries, curvature, and other quantities, for very large sets of rays. These techniques would be useful for improving the efficiency of RaySense implementations.

2. Methods

We assume all points are properly calibrated by a common preprocessing step, which can also be learned. In fact, one can use RaySense to train such a preprocessor to register the dataset. However, for simplicity, we normalize each point set to be in the unit ℓ^2 ball, with center of mass at the origin.



Figure 5: Each digit averaged over the entire data set (top) versus those sampled by RaySense (bottom).

2.1. Generating random rays

We present two ways to generate random rays. There is no *right* way to generate rays, although it is conceivable that one may find optimal ray distributions for specific applications.

Method R1 One simple approach is generating ray segments of fixed-length L , whose direction \vec{v} is uniformly sampled from the unit sphere. We add a shift \vec{a} sampled uniformly from $[-\frac{1}{2}, \frac{1}{2}]^d$ to avoid a bias for the origin. The k sample points are distributed evenly along the ray:

$$\vec{r}_i = \vec{a} + L \left(\frac{i}{k-1} - \frac{1}{2} \right) \vec{v}, \quad i = 0, \dots, k-1$$

The spacing between adjacent points on each ray is denoted by δr , which is $L/(k-1)$. We use $L = 2$.

Method R2 Another natural way to generate random rays is by random endpoints selection: choose two random points \vec{p}, \vec{q} on a sphere and connect them to form a ray. Then we evenly sample k points between \vec{p}, \vec{q} on the ray. To avoid overly short rays where information would be redundant, we use a minimum ray-length threshold τ to discard rays. Note that the distance between k sample points are different on different rays:

$$\vec{r}_i = \vec{p} + \frac{i}{k-1}(\vec{q} - \vec{p}), \quad i = 0, \dots, k-1.$$

The spacing of points on each ray varies, depending on the length of the ray segment.

Fig. 6 shows the density of rays from the ray generation methods. In this paper, we use Method R1; a fixed δr seems to help maintain spatial consistency along the rays, which increases RayNN’s classification accuracy in § 4.

2.2. What is included in the signature?

Let $f : \Gamma \times \mathbb{R}^d \mapsto X$ map points in Γ and on a ray into some “feature space” X , and assume that X is embedded in \mathbb{R}^c . Building on § 1, we generalize the RaySense signature tensor to have entries

$$[S_{m, \delta r}(\Gamma; f, \mathcal{P})]_{i,j} := f(P_{\Gamma} r_{i,j}, r_{i,j}).$$

For simplicity, we will continue to denote this RaySense signature as simply “ $S(\Gamma)$ ”.

In this work, we propose that the RaySense signature include the coordinates of the closest point to each ray sample point and the vector to the closest point:

$$f(P_{\Gamma} r_{i,j}, r_{i,j}) = [P_{\Gamma} r_{i,j}, P_{\Gamma} r_{i,j} - r_{i,j}].$$

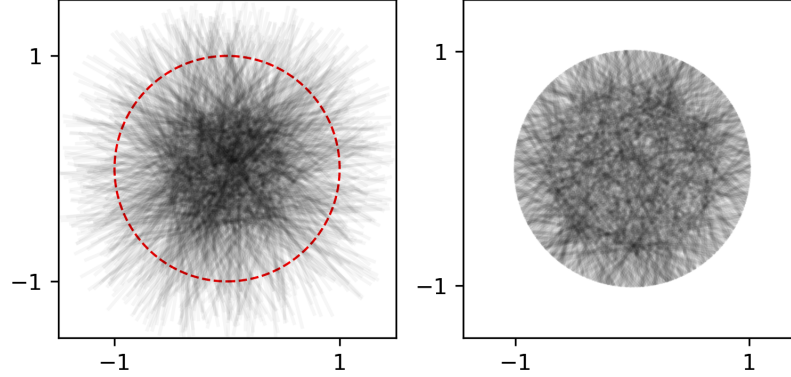


Figure 6: Density of rays from method R1 (left) and R2 (right). Red circle indicates the ℓ^2 ball.

In addition, it can include the distance to the closest point $\|P_{\Gamma}r_{i,j} - r_{i,j}\|$. The signature can also be extended to include these features from κ nearest-neighbors. We will see that incorporating additional neighbors into the signature increases robustness to outliers.

2.3. How to use $S(\Gamma)$ for classification?

A natural idea is to choose a suitable metric to define the distances between the RaySense signature tensors. Then a test data set is labeled “A” if it is closest (by the metric) to the point sets that are also labeled as “A”. We offer several choices of metric.

The Frobenius norm of the signature tensor is suitable if the signatures contain the distance and the closest point coordinates. For data sampled from smooth geometries, this information along each ray are piecewise continuous. So ℓ^2 -norm based comparison seems adequate.

Wasserstein distances are more appropriate for comparison of histograms of the RaySense data. The normalized histograms can be regarded as probability distributions. In particular, notice (Fig. 7) that RaySense histograms tend to have “spikes” that correspond to the salient points in the data set; ℓ^2 distances are not adequate for comparing distributions with such features.

Here we briefly describe the Wasserstein-1 distance, or Earth mover’s distance, that we used in this paper. Let (X, μ) and (\tilde{X}, ν) be two probability spaces and F and G be the cumulative distribution functions of μ and ν , respectively. The Wasserstein-1 distance is defined as

$$W_1(\mu, \nu) := \int_{\mathbb{R}} |F(t) - G(t)| dt.$$

Neural network classifier One can consider using a properly designed and trained *neural network*. In § 4, we present a neural network model, RayNN, for comparing point clouds in three dimensions.

3. Statistical invariances

If we collect the histogram of the points sampled from a set of randomly selected rays, we can show that the histogram has a well-defined limit as the number of rays tends to infinity. Let $U \in \mathbb{R}^d$ be a solid dimension- d ball, and $\Gamma \subsetneq U$ is a finite point set containing N distinct points. We draw random rays in \mathbb{R}^d from a distribution \mathcal{P} , e.g., by Method R1.

Let V_j denote the Voronoi cell for the j -th point, x_j in Γ , as seen in Fig. 1. Let $L_j(\omega)$ denote the length of a ray, ω , that lies in $V_j \cap U$. If ω does not intersect V_j , $L_j(\omega) := 0$. Thus, L_j is a random variable, and we denote its expectation by $\mathbb{E}[L_j]$; in other words,

$$\mathbb{E}[L_j] := \int L_j(\omega) dP(\omega).$$

A hybrid Monte-Carlo approach can approximate $\mathbb{E}[L_j]$. Draw m rays from the distribution. On each ray, collect the closest points in Γ from equidistant points that lie within U . Let δr denote the spacing between two adjacent points. Enumerate this set of points by r_i with $i \in \mathbb{Z}$. The closest point of r_i is x_j if $r_i \in V_j$. (If r_i lies on the boundary of different Voronoi cells, we pick one randomly.) Let

$$H_j(S_{m,\delta r}(\Gamma)) := \frac{1}{m} \sum_{\ell=1}^m \sum_{r_i \in V_j} \delta r.$$

Here, $S_{m,\delta r}(\Gamma)$ denotes the signature tensor. This H_j is precisely the number of times x_j is sampled by the RaySense approach, normalized by $\delta r/m$. Therefore, we arrive at the following Theorem:

Theorem 1. *Convergence of RaySensed data histograms:*

$$\lim_{\substack{m \rightarrow \infty \\ \delta r \rightarrow 0}} H_j(S_{m,\delta r}(\Gamma)) = \mathbb{E}[L_j].$$

Monte-Carlo approximations of integrals converge with a rate independent of the dimension. Consequently, for sufficiently many randomly selected rays, the histogram is essentially independent of the rays that are actually used.

Similar arguments show that the sampling of any function of the data set will be independent of the actual ray set, since the histograms are identical in the limit. More precisely, suppose $g : x \in \Gamma \mapsto \mathbb{R}$ is some function, then

$$\lim_{\substack{m \rightarrow \infty \\ \delta r \rightarrow 0}} \frac{1}{m} \sum_{\ell=1}^m \sum_{r_i \in V_j} g(x_j) \delta r = \mathbb{E}[g(x_j)L_j].$$

In Fig. 7, we show the histograms of the coordinates of the RaySensed points of Γ .

Since the Voronoi cell depends smoothly on Γ , $\mathbb{E}[L_j]$ (or $\mathbb{E}[g(x_j)L_j]$ for continuous g) will also depend smoothly on Γ . This means that it is stable against perturbation to the coordinates of the points in Γ . However, the effect of introducing new members to Γ , such as outliers, will be non-negligible. One possible way to overcome this is to use multiple nearest neighbors for points on the rays. Such information will be different for the outliers. The other possibility, as we shall demonstrate later in this paper, is to train a suitable neural network that is less sensitive to outlier contamination.

Comparison of histograms

We experiment by comparing Γ drawn from 16 384 objects of 16 categories from the ShapeNet dataset [3]. Let l^i be the label for object Γ_i . We compute the histogram h_x^i, h_y^i, h_z^i of the x, y, z coordinates, respectively, for points sampled by 50 rays with $k = 10$ samples per ray. We compare the histograms against those corresponding to other objects in the dataset, using

$$D_{i,j} = d(h_x^i, h_x^j) + d(h_y^i, h_y^j) + d(h_z^i, h_z^j),$$

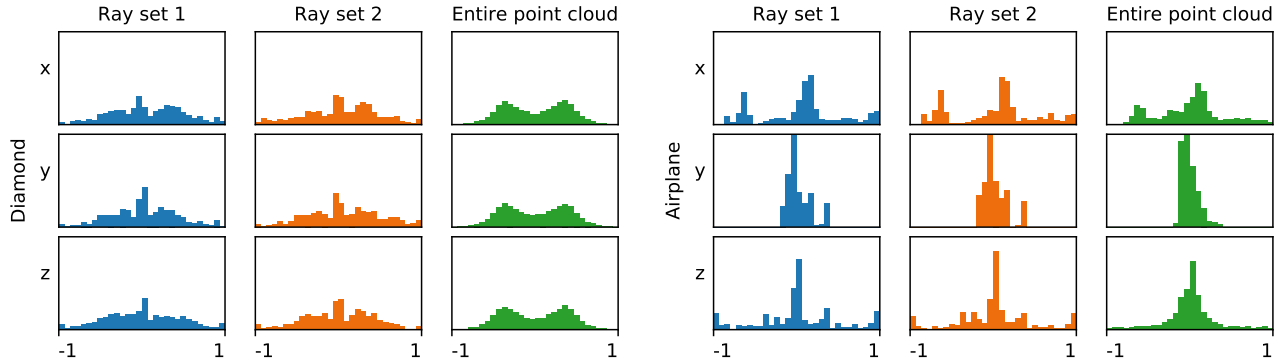


Figure 7: Histogram of coordinates from two point sets. Columns 1 and 2 correspond to 2 different sets of rays, each containing 50 rays and 50 samples per ray. These histograms are similar for the same object and different for different objects. Column 3 corresponds to the entire point cloud; these differ from the RaySense histograms.

where $d(\cdot, \cdot)$ is either the ℓ_2 or Wasserstein-1 distance. We sum D according to the respective labels

$$M_{a,b} \propto \sum_{i:l^i=a} \sum_{j:l^j=b} D_{i,j}, \quad a, b = 1, \dots, 16,$$

and normalize by the number of occurrences for each a, b pair. Fig. 8 shows the matrix of pairwise distances M between the 16 object categories.

Ideally, intra-object distances would be small, while inter-object distances would be large. As expected, Wasserstein-1 is a better metric for comparing histograms. Still, not all objects are correctly classified. When comparing histograms is not sufficient, one may consider using higher-order statistical information or neural networks to learn more complex mappings between the data and label.

4. Neural network for classification

We use the RaySense signature to classify objects from the ModelNet dataset [30], using a neural network, which we call RayNN.

We use a postfix notation to indicate more precisely what is included in the RaySense signature, see § 2.2. We use f with different number of neighbors, denoted by RayNN-X, where X is related to the input features. For our implementation, while we might use different numbers of nearest neighbors, we always include the closest point coordinates and the vector to closest points in our feature space ($c = 6$ fixed). We denote our models by RayNN- cpn where n denotes the number of nearest neighbors.

4.1. Implementation details

In this section, we provide details of RayNN. Our implementation using PyTorch [18] is available.¹

Architecture RayNN takes the $m \times k \times c$ RaySense signature tensor $S(\Gamma)$ as input, and outputs a K -vector of probabilities, where K is the number of object classes.

The first few layers of the network are blocks of 1D convolution followed by max-pooling to encode the signature into a single vector per ray. Convolution and max-pooling are applied along the ray. After

¹https://github.com/****/**** [to be added]

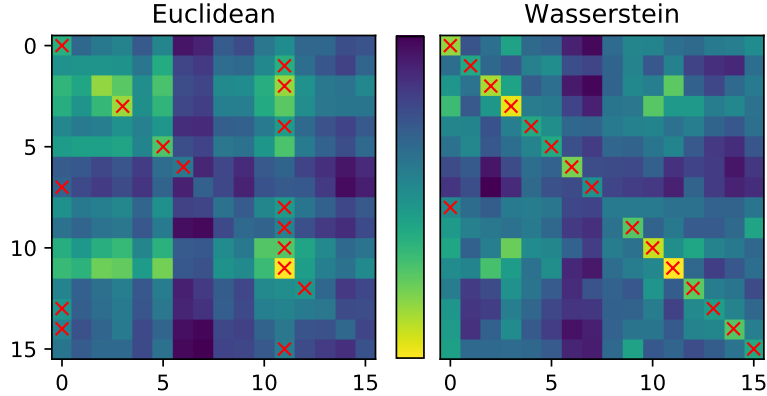


Figure 8: Comparison of histogram of the x, y, z coordinates of points sampled by RaySense, using ℓ^2 and the Wasserstein distance W_1 . Rows and columns correspond to object labels. Red \times indicate location of the argmin along each row.

this downsizing, we implement a max operation across rays. Fig. 9 includes some details. The output of the max pooling layer is fed into fully-connected layers with output sizes 256, 64, and K to produce the desired vector of probabilities $\vec{p}_i \in \mathbb{R}^K$. Batchnorm [8] along with ReLU [17] are used for every fully-connected and convolution layer.

Note that our network uses convolution along rays to capture local information while the fully-connected layers aggregate global information. Between the two, the max operation across rays ensures invariance to the ordering of the rays. It also allows for an arbitrary number of rays to be used during inference. These invariance properties are similar to PointNet’s input-order invariance [20].

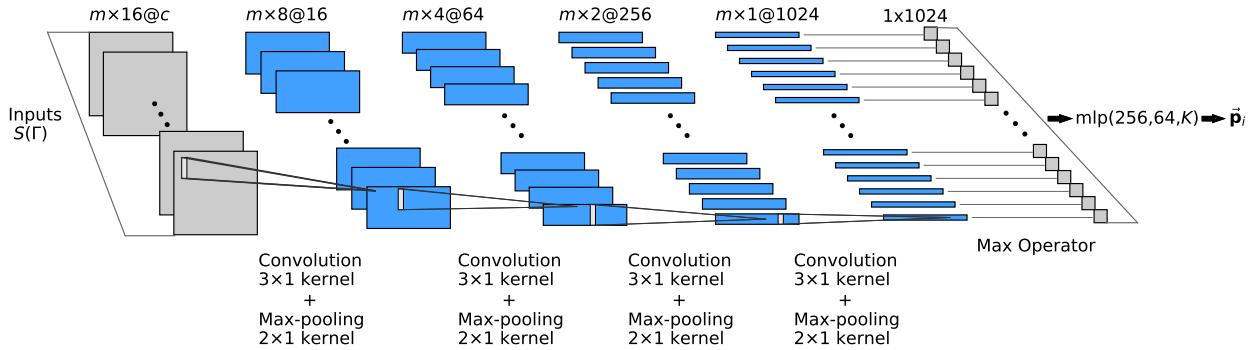


Figure 9: The RayNN architecture for m rays and k samples per ray. The input is c feature matrices from $S(\Gamma)$. With $k = 16$, each matrix is downsized to an m -vector by 4 layers of 1-D convolution and max-pooling. The max operator is then applied to each of the 1024 m -vectors. The length-1024 feature vector is fed into a multi-layer perceptron (mlp) which outputs a vector of probabilities, one for each of the K classes in the classification task. Note the number of intermediate layers (blue) can be increased based on k and c .

Data We apply RayNN on the standard ModelNet10 and ModelNet40 benchmarks [30] for 3D object classification. ModelNet40 consists of 12 311 orientation-aligned [23] meshed 3D CAD models, divided

into 9843 training and 2468 test objects. ModelNet10 contains 3991 training and 908 test objects. Following the experiment setup in [20], we sample $N = 1024$ points from each of these models and rescale them to be bounded by the unit sphere to form point sets.² Our results do not appear to be sensitive to N .

Training During training, we use dropout with ratio 0.5 on the penultimate fully-connected layer. We also augment our training dataset on-the-fly by adding $\mathcal{N}(0, 0.0004)$ noise to the coordinates. For the optimizer, we use Adam [11] with momentum 0.9 and batch size 16. The learning rate starts at 0.002 and is halved every 100 epochs.

Inference Our algorithm uses random rays, so it is natural to consider strategies to reduce the variance in the prediction. We consider one simple approach during inference by making an ensemble of predictions from λ different ray sets. The ensemble prediction is based on the average over the λ different probability vectors $\vec{p}_i \in \mathbb{R}^K$, i.e.,

$$\text{Prediction}(\lambda) = \frac{1}{\lambda} \sum_{i=1}^{\lambda} \vec{p}_i.$$

The assigned label then corresponds to the entry with the largest probability. We denote the number of rays used during training by m , while the number of rays used for inference is \hat{m} . Unless otherwise specified, we use $\lambda = 8$, $m = 32$ rays, and $\hat{m} = m$.

Table 1: ModelNet classification results. Here we report our best accuracy results over all experiments. For reference, the test scores for RayNN-cp5 ($m = 32$) has mean around 90.31% and standard deviation around 0.25% over 600 tests.

	ModelNet10	ModelNet40
PointNet [20]	–	89.2
PointNet++ [21]	–	90.7
ECC [25]	90.8	87.4
kd-net [12]	93.3	90.6
PointCNN [16]	–	92.5
PCNN [1]	94.9	92.3
DGCNN [29]	–	92.9
RayNN-cp1 ($m = 16$)	94.05	90.84
RayNN-cp5 ($m = 32$)	95.04	90.96

4.2. RayNN Results

We compare with some state-of-the-art methods for 3D point cloud classification tasks. In addition to the results reported by [20], we also compare against PointNet.pytorch, a PyTorch reimplementation [5] of PointNet. In all our experiments, we report overall accuracy. Table 1 shows RayNN is competitive. To investigate the robustness of our network, we perform several more experiments.

Robustness to sample size We repeat the experiments in [20, 29] whereby, after training, data is randomly removed prior to testing on the remaining points. The results in Fig. 10 show that RayNN performs very well with significant missing data.

²RaySense does not require point clouds for inputs: we could apply RaySense directly to surface meshes, implicit surfaces, or even—given an fast nearest neighbor calculator—the CAD models directly.

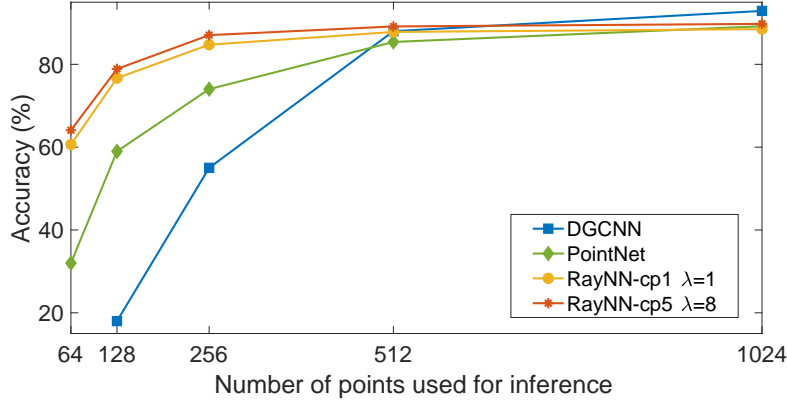


Figure 10: Testing DGCNN [29], PointNet [20] and RayNN on ModelNet40 with missing data.

Table 2: Accuracy when testing with a reduced ray set. RayNN-cp1 was trained using $m = 32$ rays. Results averaged over 5 runs.

ModelNet40				
\hat{m}	32	16	8	4
$\lambda = 1$	88.50%	86.13%	74.64%	43.28%
$\lambda = 8$	89.77%	88.94%	82.97%	55.24%

Using fewer rays We experiment with training using a full set of $m = 32$ rays but test using smaller number \hat{m} of rays. Table 2 shows that RayNN can achieve a reasonable score even if only $\hat{m} = 4$ rays are used for inference.

Robustness to outliers This experiment simulates situations where noise severely perturbs the original data during testing. We compare the performance of RayNN-cp1, RayNN-cp5 and PointNet.pytorch in Table 3. The comparison reveals RaySense’s capability in handling unexpected outliers, especially when additional nearest neighbors are used. Note the experiment here is different from that in [20] where the outliers are fixed and included in the training set.

4.3. Complexity analysis

Table 4 shows that our network has an advantage in model size and feedforward time even against the simple and efficient PointNet. In both training and testing, there is some overhead in data preprocessing to build a kd-tree, generate rays, and perform the nearest-neighbour queries to form the RaySense signature. For point clouds of around $N = 1024$, these costs are not too onerous in practice as shown in table 4.

The convolution layers have $48c + 840016$ parameters, where c is the dimension of input feature space. The fully-connected layers have $64K + 278528$ parameters, where K is the number of output classes. In total, our network has $1.1 \times 10^6 + 48c + 64K \approx 1.1\text{M}$ parameters. In comparison, PointNet [20] contains 3.5M parameters.

Table 3: Outliers sampled uniformly from the unit sphere are introduced during testing. The networks are trained without any outliers. Results averaged over 5 runs.

ModelNet10	no outliers	5 outliers	10 outliers
RayNN-cp1	93.26%	79.76%	53.94%
RayNN-cp5	93.85%	92.66%	90.90%
PointNet.pytorch	91.08%	48.57%	25.55%
ModelNet40			
RayNN-cp1	89.77 %	54.66%	20.95%
RayNN-cp5	90.38%	88.49%	78.06%
PointNet.pytorch	87.15%	34.05%	17.48%

5. Conclusions and discussions

RaySense is a data sampling technique based on projecting random rays onto a data set. The projection is done by finding nearest neighbors in the data for each point along the ray. These nearest neighbors—augmented with additional features—form the “RaySense signature”, which can be used for data processing tasks.

RaySense samples salient features of the data set, such as corners or edges, with higher probability. From the RaySense signature, local information can be recovered. However, nearest-neighbor information is sensitive to outliers; using multiple nearest neighbors enhances RaySense’s capability to capture persistent features in the data set, thereby improving robustness.

We have shown theoretically that the statistics of a sampled point cloud depends only on the distribution of the rays, but not on a particular ray set. While we focus here mostly on three-dimensional point clouds, we have also demonstrated a few experiments studying RaySense in higher dimensions. The complexity of RaySense involves the numerical resolution of a single ray and Monte-Carlo sampling of the ray-distribution. The product of these is suggestive of independence of the dimension of the data embedding space. Our experience with three-dimensional data indicates not too many rays are needed in practice.

For classification of point clouds in three dimensions, we presented a neural network classifier called “RayNN” which takes the RaySense signatures as input. We compared its performance to several other prominent models. RayNN is lightweight, flexible, efficient, and different from conventional models; for the same data set, one can test multiple times with different ray sets.

To the best of our knowledge RaySense is a new idea, so there are many avenues of possible study. On the theoretical side, one could study RaySense’s invariant properties for more general geometric objects beyond point clouds. and its connections to topological structure. There are many practical applications to explore such as training with outliers or the simultaneous registration, classification and segmentation of point clouds. Finally, we expect to find applications to high-dimensional data sets. For example, RaySense could be used as intermediate step for the semi-guided identification of appropriate feature spaces.

Acknowledgments We acknowledge Albert Chern for useful discussions. Part of this research was performed while the second author was visiting the Institute for Pure and Applied Mathematics (IPAM), which is supported by the National Science Foundation (Grant No. DMS-1440415). This work was partially supported by a grant from the Simons Foundation and NSF Grant DMS-1720171. The authors

Table 4: Top: storage and timings for RayNN-cp1 and PointNet.pytorch on ModelNet40 using one Nvidia 1080-Ti GPU. The preprocessing time is measured per object. And RayNN uses batch size 32 here for forward time comparison. Bottom: data from [29] is included only for reference; no proper basis for direct comparison.

	Model size	Forward time	Preprocessing time	Time per epoch
PointNet.pytorch	14 MB	12 ms	3.6 ms	14 s
RayNN-cp1	4.5 MB	2 ms	7.5 ms	22 s
PointNet [20]	40 MB	16.6 ms	-	-
PCNN [1]	94 MB	117 ms	-	-
DGCNN [29]	21 MB	27.2 ms	-	-

thank Texas Advanced Computing Center (TACC) for providing computing resources.

References

- [1] Matan Atzmon, Haggai Maron, and Yaron Lipman. Point convolutional neural networks by extension operators. *arXiv preprint arXiv:1803.10091*, 2018. [5](#), [11](#), [14](#)
- [2] Jon Louis Bentley. Multidimensional binary search trees used for associative searching. *Commun. ACM*, 1975. [1](#)
- [3] Angel X Chang, Thomas Funkhouser, Leonidas Guibas, Pat Hanrahan, Qixing Huang, Zimo Li, Silvio Savarese, Manolis Savva, Shuran Song, Hao Su, et al. Shapenet: An information-rich 3D model repository. *arXiv preprint arXiv:1512.03012*, 2015. [1](#), [8](#)
- [4] Yi Fang, Jin Xie, Guoxian Dai, Meng Wang, Fan Zhu, Tiantian Xu, and Edward Wong. 3D deep shape descriptor. In *Proceedings of the IEEE Conference on Computer Vision and Pattern Recognition*, pages 2319–2328, 2015. [4](#)
- [5] Fei Xia and others. Pointnet.pytorch git repository. <https://github.com/fxia22/pointnet.pytorch>. [11](#)
- [6] Hugo Hadwiger. *Vorlesungen über inhalt, Oberfläche und isoperimetrie*, volume 93. Springer-Verlag, 2013. [4](#)
- [7] Markus Hadwiger, Christian Sigg, Henning Scharsach, Khatja Bhler, and Markus Gross. Real-time ray-casting and advanced shading of discrete isosurfaces. *Computer Graphics Forum*, 2005. [5](#)
- [8] Sergey Ioffe and Christian Szegedy. Batch normalization: Accelerating deep network training by reducing internal covariate shift. *arXiv preprint arXiv:1502.03167*, 2015. [10](#)
- [9] Peter Wilcox Jones, Andrei Osipov, and Vladimir Rokhlin. Randomized approximate nearest neighbors algorithm. *Proc. Natl. Acad. Sci.*, 2011. [1](#)
- [10] Ismail Khalid Kazmi, Lihua You, and Jian Jun Zhang. A survey of 2D and 3D shape descriptors. In *2013 10th International Conference Computer Graphics, Imaging and Visualization*, pages 1–10. IEEE, 2013. [4](#)
- [11] Diederik P Kingma and Jimmy Ba. Adam: A method for stochastic optimization. *arXiv preprint arXiv:1412.6980*, 2014. [11](#)
- [12] Roman Klokov and Victor Lempitsky. Escape from cells: Deep KD-networks for the recognition of 3D point cloud models. In *Proceedings of the IEEE International Conference on Computer Vision*, pages 863–872, 2017. [5](#), [11](#)

- [13] Scott Krig. Interest point detector and feature descriptor survey. In *Computer vision metrics*, pages 187–246. Springer, 2016. 5
- [14] J. Kruger and R. Westermann. Acceleration techniques for gpu-based volume rendering. In *IEEE Visualization VIS 2003.*, 2003. 5
- [15] Yann LeCun. The mnist database of handwritten digits. <http://yann.lecun.com/exdb/mnist/>, 1998. 3
- [16] Yangyan Li, Rui Bu, Mingchao Sun, Wei Wu, Xinhan Di, and Baoquan Chen. Pointcnn: Convolution on x-transformed points. In *Advances in Neural Information Processing Systems*, pages 820–830, 2018. 5, 11
- [17] Vinod Nair and Geoffrey E Hinton. Rectified linear units improve restricted boltzmann machines. In *Proceedings of the 27th international conference on machine learning (ICML-10)*, pages 807–814, 2010. 10
- [18] Adam Paszke, Sam Gross, Soumith Chintala, Gregory Chanan, Edward Yang, Zachary DeVito, Zeming Lin, Alban Desmaison, Luca Antiga, and Adam Lerer. Automatic differentiation in PyTorch. In *NIPS Autodiff Workshop*, 2017. 9
- [19] Jon Peddie. *Ray Tracing: A Tool for All*. Springer, 2019. 5
- [20] Charles R Qi, Hao Su, Kaichun Mo, and Leonidas J Guibas. Pointnet: Deep learning on point sets for 3d classification and segmentation. In *Proceedings of the IEEE Conference on Computer Vision and Pattern Recognition*, pages 652–660, 2017. 5, 10, 11, 12, 14
- [21] Charles Ruizhongtai Qi, Li Yi, Hao Su, and Leonidas J Guibas. Pointnet++: Deep hierarchical feature learning on point sets in a metric space. In *Advances in neural information processing systems*, pages 5099–5108, 2017. 5, 11
- [22] Reihaneh Rostami, Fereshteh S Bashiri, Behrouz Rostami, and Zeyun Yu. A survey on data-driven 3D shape descriptors. *Comput. Graph. Forum*, 38(1):356–393, 2019. 4
- [23] Nima Sedaghat, Mohammadreza Zolfaghari, Ehsan Amiri, and Thomas Brox. Orientation-boosted voxel nets for 3d object recognition. *arXiv preprint arXiv:1604.03351*, 2016. 10
- [24] Burr Settles. Active learning literature survey. Technical report, University of Wisconsin-Madison Department of Computer Sciences, 2009. 4
- [25] Martin Simonovsky and Nikos Komodakis. Dynamic edge-conditioned filters in convolutional neural networks on graphs. In *Proceedings of the IEEE conference on computer vision and pattern recognition*, pages 3693–3702, 2017. 5, 11
- [26] Ayan Sinha, Jing Bai, and Karthik Ramani. Deep learning 3d shape surfaces using geometry images. In *European Conference on Computer Vision*. Springer, 2016. 4
- [27] Yen-Hsi Richard Tsai. Rapid and accurate computation of the distance function using grids. *J. Comput. Phys.*, 2002. 1
- [28] Peng-Shuai Wang, Yang Liu, Yu-Xiao Guo, Chun-Yu Sun, and Xin Tong. O-cnn: Octree-based convolutional neural networks for 3d shape analysis. *ACM Transactions on Graphics (TOG)*, 36(4):72, 2017. 5
- [29] Yue Wang, Yongbin Sun, Ziwei Liu, Sanjay E Sarma, Michael M Bronstein, and Justin M Solomon. Dynamic graph cnn for learning on point clouds. *ACM Transactions on Graphics (TOG)*, 38(5):146, 2019. 5, 11, 12, 14
- [30] Zhirong Wu, Shuran Song, Aditya Khosla, Fisher Yu, Linguang Zhang, Xiaoou Tang, and Jianxiong Xiao. 3d shapenets: A deep representation for volumetric shapes. In *Proceedings of the IEEE conference on computer vision and pattern recognition*, pages 1912–1920, 2015. 1, 9, 10
- [31] Jin Xie, Guoxian Dai, Fan Zhu, Edward K Wong, and Yi Fang. Deepshape: Deep-learned shape descriptor for 3d shape retrieval. *IEEE transactions on pattern analysis and machine intelligence*, 39(7):1335–1345, 2016. 4

- [32] Yin Zhou and Oncel Tuzel. Voxelnet: End-to-end learning for point cloud based 3d object detection. In *Proceedings of the IEEE Conference on Computer Vision and Pattern Recognition*, pages 4490–4499, 2018.